Article

Exploring Anisotropic Lorentz Invariance Violation from the Spectral-Lag Transitions of Gamma-Ray Bursts

Jin-Nan Wei [1,2,3]**, Zi-Ke Liu** [4,5]**, Jun-Jie Wei** [1,2,3,*]**, Bin-Bin Zhang** [4,5] **and Xue-Feng Wu** [1,2]

1   Purple Mountain Observatory, Chinese Academy of Sciences, Nanjing 210023, China
2   School of Astronomy and Space Sciences, University of Science and Technology of China, Hefei 230026, China
3   Guangxi Key Laboratory for Relativistic Astrophysics, Nanning 530004, China
4   School of Astronomy and Space Science, Nanjing University, Nanjing 210023, China
5   Key Laboratory of Modern Astronomy and Astrophysics (Nanjing University), Ministry of Education, Nanjing 210023, China
*   Correspondence: jjwei@pmo.ac.cn

Abstract: The observed spectral lags of gamma-ray bursts (GRBs) have been widely used to explore possible violations of Lorentz invariance. However, these studies were generally performed by concentrating on the rough time lag of a single highest-energy photon and ignoring the intrinsic time lag at the source. A new way to test nonbirefringent Lorentz-violating effects has been proposed by analyzing the multi-photon spectral-lag behavior of a GRB that displays a positive-to-negative transition. This method gives both a plausible description of the intrinsic energy-dependent time lag and comparatively robust constraints on Lorentz-violating effects. In this work, we conduct a systematic search for Lorentz-violating photon dispersion from the spectral-lag transition features of 32 GRBs. By fitting the spectral-lag data of these 32 GRBs, we place constraints on a variety of isotropic and anisotropic Lorentz-violating coefficients with mass dimension $d = 6$ and 8. While our dispersion constraints are not competitive with existing bounds, they have the promise to complement the full coefficient space.

Keywords: gamma-ray bursts; astroparticle physics; gravitation; quantum gravity

1. Introduction

Lorentz invariance, the foundational symmetry of Einstein's relativity, has survived in a wide range of tests over the past century [1]. However, many quantum gravity models seeking to unify general relativity and quantum theory predict that Lorentz symmetry may be violated at energies approaching the Planck scale $E_{\rm Pl} = \sqrt{\hbar c^5/G} \simeq 1.22 \times 10^{19}$ GeV [2–9]. While these energies are unreachable experimentally, tiny deviations from Lorentz invariance at attainable energies can accumulate to detectable levels over sufficiently large distances. Astrophysical observations involving long propagation distances can therefore provide precision tests of Lorentz invariance.

In the photon sector, one effect of Lorentz invariance violation (LIV) is an energy-dependent vacuum dispersion of light, which causes arrival-time delays of photons with different energies originating from a given astrophysical source [10–26]. LIV models can also lead to vacuum birefringence, which produces an energy-dependent rotation of the polarization vector of linearly polarized light [27–38]. Generally, these effects can be anisotropic, such that arrival-time differences and polarization rotations possess a direction dependence and require observations of point sources along many lines of sight or measurements of extended sources such as the cosmic microwave background to fully explore the LIV model parameter space [15,16,36].

The Standard-Model Extension (SME) is an effective field theory that characterizes Lorentz and CPT violations at attainable energies [39–41]. It considers additional Lorentz and/or CPT-violating terms to the SME Lagrange density, which can be ordered by the mass

dimension d of the tensor operator [16]. Photon vacuum dispersion introduced by operators of dimension d ($\neq 4$) is proportional to $(E/E_{\mathrm{Pl}})^{d-4}$. Lorentz-violating operators with even d preserve CPT symmetry, while those with odd d break CPT. All $(d-1)^2$ coefficients of odd d produce both vacuum dispersion and birefringence, whereas for each even d there is a subset of $(d-1)^2$ nonbirefringent but dispersive Lorentz-violating coefficients. The latter can be well constrained through vacuum dispersion time-of-flight measurements. It should be stressed that at least $(d-1)^2$ sources distributed evenly in the sky are needed to fully constrain the anisotropic Lorentz-violating coefficient space for a given d. In contrast, only one source is required to fully constrain the corresponding coefficient in the isotropic LIV limit. That is, the restriction to isotropic LIV disregards $d(d-2)$ possible effects from anisotropic violations at each d.

Thanks to their small variability time scales, large cosmological distances, and very high-energy photons, gamma-ray bursts (GRBs) are viewed as one of the ideal probes for testing Lorentz invariance through the dispersion method [10,13,14]. Direction-dependent limits on several combinations of coefficients for Lorentz violation have been placed using vacuum-dispersion constraints from GRBs. For example, limits on combinations of the 25 $d = 6$ nonbirefringent Lorentz-violating coefficients have been derived by studying the dispersion of light in observations of GRB 021206 [15,42], GRB 080916C [16,17], four bright GRBs [19], GRB 160625B [22], and GRB 190114C [24]. Bounds on combinations of the 49 $d = 8$ coefficients for nonbirefringent vacuum dispersion have been derived from GRB 021206 [15,42], GRB 080916C [16,17], GRB 160625B [22], and GRB 190114C [24]. However, most of these studies limit attention to the time delay induced by nonbirefringent Lorentz-violating effects, while ignoring possible source-intrinsic time delays. Furthermore, the limits from GRBs are based on the rough time delay of a single highest-energy photon. To obtain reliable LIV limits, it is desirable to use the true time lags of high-quality and high-energy light curves in different energy multi-photon bands.

In two previous papers [22,24], we derived new direction-dependent limits on combinations of coefficients for Lorentz-violating vacuum dispersion using the peculiar time-of-flight measurements of GRB 160625B and GRB 190114C, which both have obvious transitions from positive to negative spectral lags. Spectral lag, which is defined as the arrival-time difference of high- and low-energy photons, is a ubiquitous feature in GRBs [43–45]. Conventionally, the spectral lag is considered to be positive when high-energy photons arrive earlier than the low-energy ones. By fitting the spectral-lag behaviors of GRB 160625B and GRB 190114C, we obtained both a reasonable formulation of the intrinsic energy-dependent time lag and robust constraints on a variety of isotropic and anisotropic Lorentz-violating coefficients with mass dimension $d = 6$ and 8 [22,24]. In this work, we analyze the spectral-lag transition features of 32 *Fermi* GRBs [25], and derive limits on photon vacuum dispersion for all of them. We combine these limits with previous results in order to fully constrain the nonbirefringent Lorentz-violating coefficients with $d = 6$ and 8.

The paper is structured as follows. In Section 2, we briefly describe the theoretical framework of vacuum dispersion in the SME. In Section 3, we introduce our analysis method, and then present our resulting constraints on the Lorentz-violating coefficients. The physical implications of our results are discussed in Section 4. Finally, we summarize our main conclusions in Section 5.

2. Theoretical Framework

In the SME framework, the LIV-induced modifications to the photon dispersion relation can be described in the form [15,16]

$$E(p) \simeq \left(1 - \varsigma^0 \pm \sqrt{(\varsigma^1)^2 + (\varsigma^2)^2 + (\varsigma^3)^2}\right) p \,, \qquad (1)$$

where p is the photon momentum. The symbols $\varsigma^0, \varsigma^1, \varsigma^2$, and ς^3 are the combinations of coefficients for LIV that depend on the momentum and direction of propagation. These four combinations can be decomposed on a spherical harmonic basis to yield

$$\varsigma^0 = \sum_{djm} p^{d-4} {}_0Y_{jm}(\hat{\boldsymbol{n}}) c^{(d)}_{(I)jm},$$

$$\varsigma^1 \pm i\varsigma^2 = \sum_{djm} p^{d-4} {}_{\mp 2}Y_{jm}(\hat{\boldsymbol{n}}) \left(k^{(d)}_{(E)jm} \mp i k^{(d)}_{(B)jm} \right), \tag{2}$$

$$\varsigma^3 = \sum_{djm} p^{d-4} {}_0Y_{jm}(\hat{\boldsymbol{n}}) k^{(d)}_{(V)jm},$$

where $\hat{\boldsymbol{n}}$ is the direction of the source and ${}_sY_{jm}(\hat{\boldsymbol{n}})$ represents spin-weighted harmonics of spin weight s. The coordinates (θ, ϕ) of $\hat{\boldsymbol{n}}$ are in a Sun-centered celestial-equatorial frame [46], such that $\theta = (90° - \text{Dec.})$ and $\phi = \text{R.A.}$, where R.A. and Dec. are the right ascension and declination of the astrophysical source, respectively.

With the above decomposition, all types of LIV for vacuum propagation can be characterized using four sets of spherical coefficients: $c^{(d)}_{(I)jm}$, $k^{(d)}_{(E)jm}$, and $k^{(d)}_{(B)jm}$ for CPT-even effects and $k^{(d)}_{(V)jm}$ for CPT-odd effects. For each coefficient, the relevant Lorentz-violating operator has mass dimension d and eigenvalues of total angular momentum written as jm. The coefficients $c^{(d)}_{(I)jm}$ are associated with CPT-even operators causing dispersion without leading-order birefringence, while nonzero coefficients $k^{(d)}_{(E)jm}$, $k^{(d)}_{(B)jm}$, and $k^{(d)}_{(V)jm}$ produce birefringence. In the present work, we focus on the nonbirefringent vacuum dispersion coefficients $c^{(d)}_{(I)jm}$. Setting all other coefficients for birefringent propagation to zero, the group-velocity defect including anisotropies is given by

$$\delta v_g = -\sum_{djm} (d-3) E^{d-4} {}_0Y_{jm}(\hat{\boldsymbol{n}}) c^{(d)}_{(I)jm}, \tag{3}$$

in terms of the photon energy E. Note that the factor $(d-3)$ refers to the difference between group and phase velocities [22]. For even $d \geq 6$, nonzero values of $c^{(d)}_{(I)jm}$ imply an energy-dependent vacuum dispersion of light, so two photons with different energies $(E_h > E_l)$ emitted simultaneously from the same astrophysical source at redshift z would be observed at different times. The arrival-time difference can therefore be derived as [15]

$$\begin{aligned}
\triangle t_{\text{LIV}} &= t_l - t_h \\
&\approx -(d-3)\left(E_h^{d-4} - E_l^{d-4} \right) \int_0^z \frac{(1+z')^{d-4}}{H(z')} dz' \sum_{jm} {}_0Y_{jm}(\hat{\boldsymbol{n}}) c^{(d)}_{(I)jm},
\end{aligned} \tag{4}$$

where t_l and t_h are the arrival times of photons with observed energies E_l and E_h, respectively. In the flat ΛCDM model, the Hubble expansion rate $H(z)$ is expressed as $H(z) = H_0 \left[\Omega_m (1+z)^3 + \Omega_\Lambda \right]^{1/2}$, where $H_0 = 67.36$ km s^{-1} Mpc^{-1} is the Hubble constant, $\Omega_m = 0.315$ is the matter density, and $\Omega_\Lambda = 1 - \Omega_m$ is the cosmological constant energy density [47]. In the SME case of a direction-dependent LIV, we constrain the combination $\sum_{jm} {}_0Y_{jm}(\hat{\boldsymbol{n}}) c^{(d)}_{(I)jm}$ as a whole. For the limiting case of the vacuum isotropic model $(j = m = 0)$, all the terms in the combination become zero except ${}_0Y_{00} = Y_{00} = \sqrt{1/(4\pi)}$. In that case, we constrain a single $c^{(d)}_{(I)00}$ coefficient.

3. Constraints on Anisotropic LIV

By systematically analyzing the spectral lags of 135 *Fermi* long GRBs with redshift measurement, Liu et al. [25] identified 32 of them having well-defined transitions from

positive to negative spectral lags. For each GRB, Liu et al. [25] extracted its multi-band light curves and calculated the spectral time lags for any pair of light curves between the lowest-energy band and any other higher-energy bands. In Figure 1, we plot the time lags of each burst as a function of energy. One can see that all GRBs exhibit a positive-to-negative lag transition. In this section, we utilize the spectral-lag transitions of these 32 GRBs to pose direction-dependent constraints on combinations of nonbirefringent Lorentz-violating coefficients $c_{(I)jm}^{(6)}$ and $c_{(I)jm}^{(8)}$. The 32 GRBs used in our study are listed in Table 1, which includes the following information for each burst: its name, the right ascension coordinate, the declination coordinate, and the redshift z.

Table 1. List of 32 GRBs with spectral-lag transitions.

Name	R.A. J2000 [°]	Dec. J2000 [°]	Redshift z [1]	Ref. [2]
GRB 080916C	119.8	−56.6	4.35	[48]
GRB 081221	15.8	−24.5	2.26	[48]
GRB 090328	155.7	+33.4	0.736	[48]
GRB 090618	294.0	+78.4	0.54	[48]
GRB 090926A	353.4	−66.3	2.1062	[48]
GRB 091003A	251.5	−36.6	0.8969	[48]
GRB 100728A	88.8	−15.3	1.567	[48]
GRB 120119A	120.0	−9.8	1.728	[48]
GRB 130427A	173.1	+27.7	0.3399	[48]
GRB 130518A	355.7	+47.5	2.488	[48]
GRB 130925A	41.2	−26.1	0.347	[48]
GRB 131108A	156.5	+9.7	2.40	[48]
GRB 131231A	10.6	−1.6	0.642	[48]
GRB 140206A	145.3	+66.8	2.73	[48]
GRB 140508A	255.5	+46.8	1.027	[48]
GRB 141028A	322.6	−0.2	2.33	[48]
GRB 150314A	126.7	+63.8	1.758	[48]
GRB 150403A	311.5	−62.7	2.06	[48]
GRB 150514A	74.8	−60.9	0.807	[48]
GRB 150821A	341.9	−57.9	0.755	[48]
GRB 160509A	310.1	+76.0	1.17	[48]
GRB 160625B	308.6	+6.9	1.41	[48]
GRB 171010A	66.6	−10.5	0.3285	[48]
GRB 180703A	6.5	−67.1	0.6678	[48]
GRB 180720B	0.59	−3.0	0.654	[49]
GRB 190114C	54.5	−26.9	0.425	[50]
GRB 200613A	153.0	+45.8	1.22	[51]
GRB 200829A	251.1	+72.4	1.25	[52]
GRB 201216C	16.4	+16.5	1.10	[53]
GRB 210204A	109.1	+9.7	0.876	[54]
GRB 210610B	243.9	+14.4	1.13	[55]
GRB 210619B	319.7	+33.9	1.937	[56]

[1] All source redshifts were obtained from Liu et al. [25] and references therein. [2] Individual references are given for the coordinates.
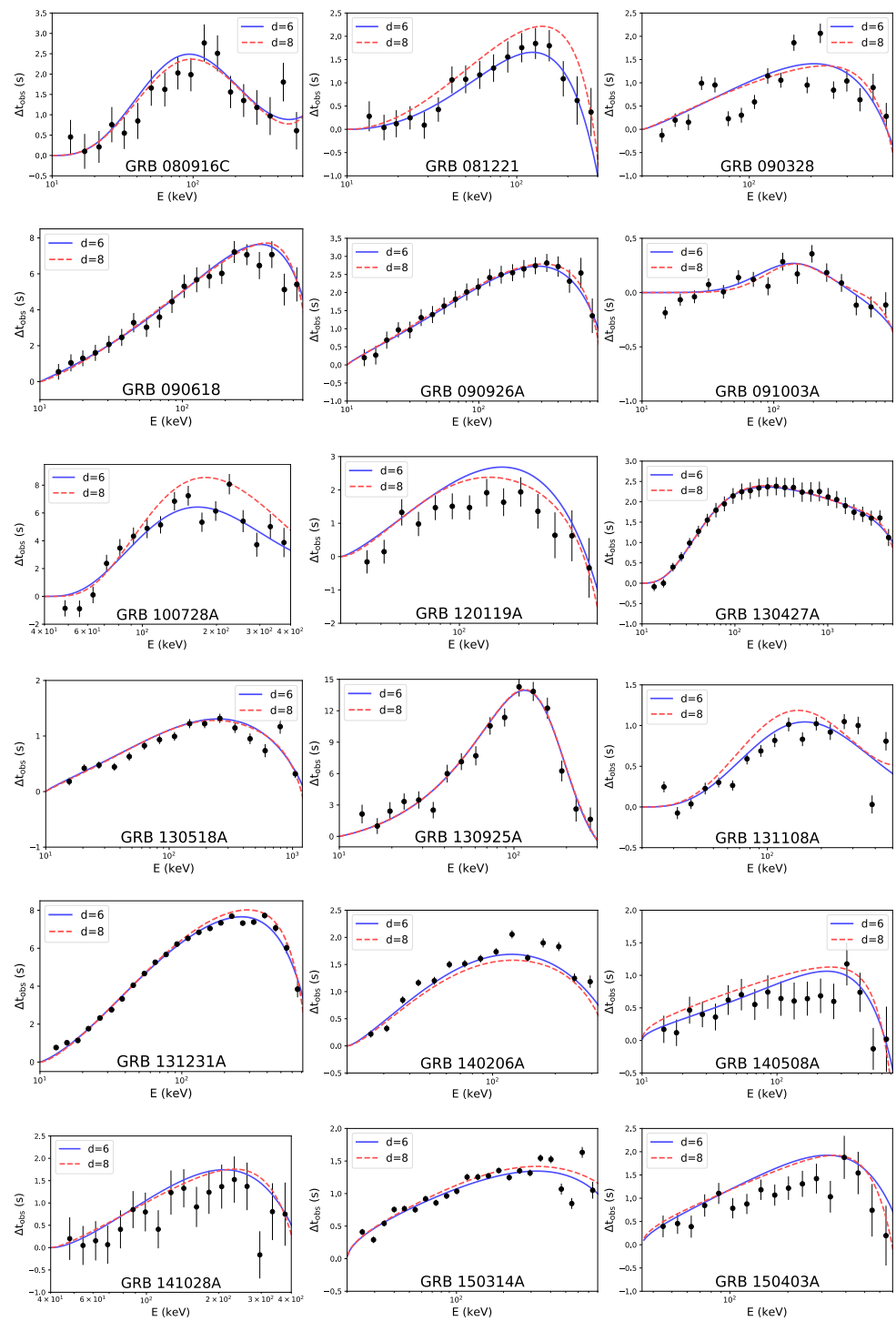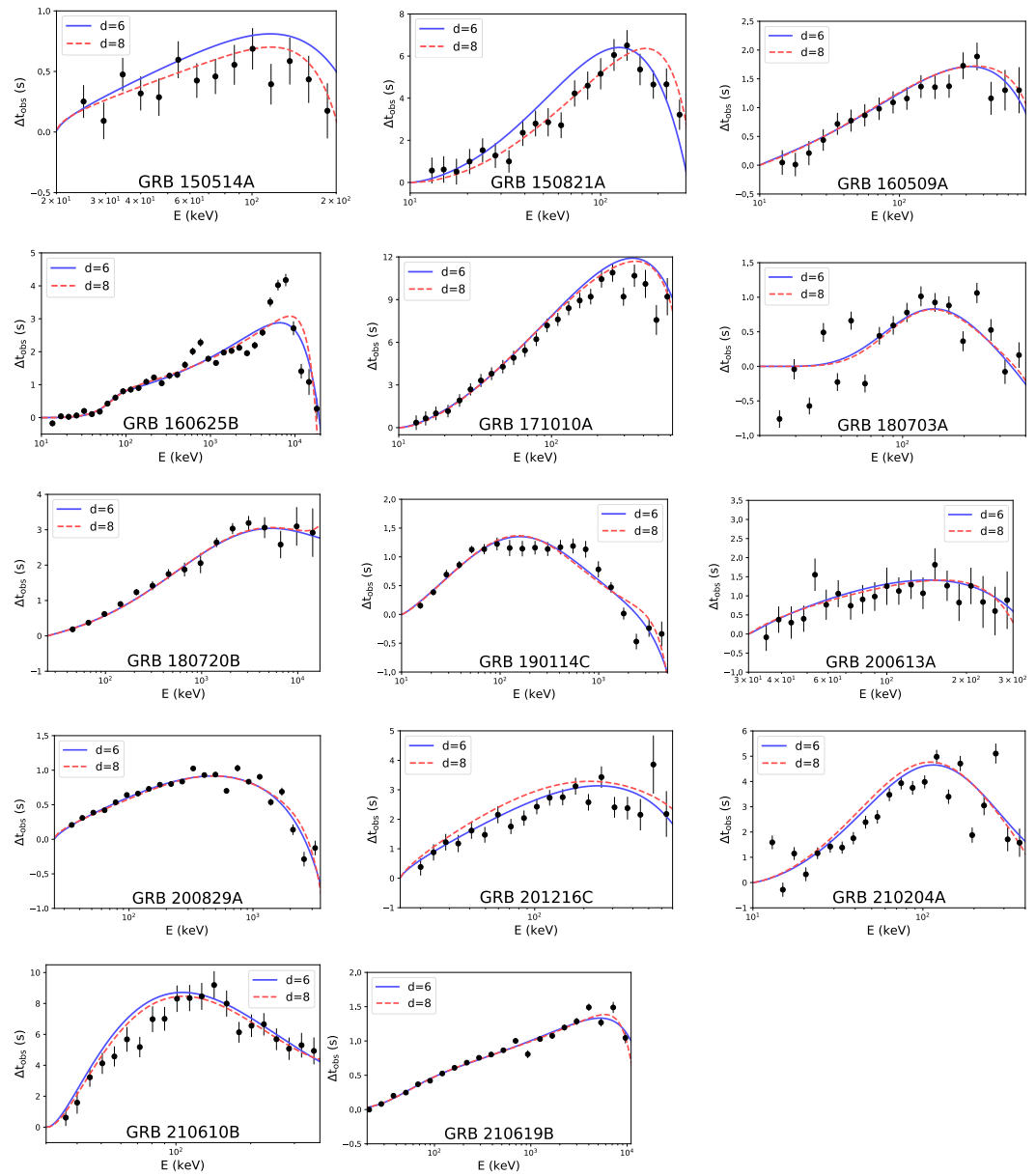
Figure 1. *Cont.*

Figure 1. Energy dependence of the observed spectral lag Δt_{obs} of each GRB in our sample, and the best-fit theoretical curves. Blue solid lines: model with $d = 6$ coefficients. Red dashed lines: model with $d = 8$ coefficients.

In view of the LIV-induced time delay, Δt_{LIV} is likely to be accompanied by an intrinsic time delay Δt_{int} caused by the emission mechanism of GRBs [13,21,22,57]; the observed spectral lag should consist of two terms

$$\Delta t_{\mathrm{obs}} = \Delta t_{\mathrm{int}} + \Delta t_{\mathrm{LIV}} \ . \tag{5}$$

In principle, it is hard to model the intrinsic lag behavior because of the unknown GRB emission mechanism. As previous works have excluded some nonbirefringent Lorentz-violating effects with a high level of confidence (e.g., [19]), it is reasonable to assume that the observed spectral lag is dominated by the intrinsic time lag, and the LIV-induced time lag is negligible. Statistically, the time lags of these 32 GRBs first increase and then decrease with the energies in the form of an approximate broken power-law function, i.e., the broken power-law model is in fact an accurate representation of the energy dependence of the intrinsic time lag. Hence, as Liu et al. [25] conducted in their treatment, we adopt a

smoothly broken power-law (SBPL) function to model the intrinsic energy-dependent time lag,

$$\Delta t_{\text{int}} = \tau \left(\frac{E - E_l}{E_b} \right)^{\alpha_1} \left\{ \frac{1}{2} \left[1 + \left(\frac{E - E_l}{E_b} \right)^{1/\beta} \right] \right\}^{(\alpha_2 - \alpha_1)\beta}, \tag{6}$$

where τ is the normalization amplitude, E_l is the median value of the lowest energy band of each GRB, α_1 and α_2 are the power-law indices before and after the break energy E_b, and β measures the smoothness of the transition. In order to ensure that Δt_{int} is consistent with the observed lag behavior displaying a transition from positive to negative lags, we require the Δt_{LIV} term in Equation (5) not to dominate over Δt_{int}. That is, we require $\alpha_1 \geq \alpha_2$.

We fit the lag-energy measurements of each GRB using the theoretical model as shown in Equations (4)–(6). The free parameters (τ, α_1, α_2, E_b, and β) of the SBPL function and the combination $\sum_{jm} {}_0 Y_{jm}(\hat{n}) c^{(d)}_{(I)jm}$ of SME coefficients are simultaneously estimated by using the Markov chain Monte Carlo (MCMC) technique. The Python MCMC module EMCEE [58] is adopted to explore the posterior probability distributions of these parameters. The log-likelihood sampled by EMCEE is given by

$$\ln L(\theta) = -\frac{1}{2} \sum_i \frac{[\Delta t_{\text{obs},i} - \Delta t_{\text{model}}(\theta)]^2}{\sigma^2_{\Delta t_{\text{obs},i}}}, \tag{7}$$

where $\sigma_{\Delta t_{\text{obs},i}}$ is the uncertainty of the ith lag measurement $\Delta t_{\text{obs},i}$, $\Delta t_{\text{model}}(\theta)$ is obtained from Equation (5), and θ denotes the free parameters. In our analysis, we choose wide flat priors for $\tau \in [0.0, 4.0]$ s, $\alpha_1 \in [-3.0, 10.0]$, $\alpha_2 \in [-10.0, 3.0]$, $\beta \in [0.0, 3.0]$, and $E_b \in [0.0, 5000.0]$ keV. The prior of the combination $\sum_{jm} {}_0 Y_{jm}(\hat{n}) c^{(d)}_{(I)jm}$ of SME coefficients is set as a uniform distribution in the range of $[-10^{-10}, 10^{-10}]$ GeV^{-2} for $d = 6$, or $[-10^{-3}, 10^{-3}]$ GeV^{-4} for $d = 8$. Note that the spectral-lag transition from positive to negative is for the power-law indices (α_1 and α_2) when fitting the observed lag-energy data.

The resulting constraints from the observed lag-energy data of each GRB are presented in Table 2. For each value $d = 6, 8$ in turn, the best-fit results and 2σ uncertainties are provided for the parameters τ, α_1, α_2, and E_b and for the direction-dependent combination $\sum_{jm} {}_0 Y_{jm}(\hat{n}) c^{(d)}_{(I)jm}$ of Lorentz-violating coefficients. Table 2 also provides estimated constraints at the 95% confidence level for the corresponding coefficients in the restrictive isotropic limit $j = m = 0$. To illustrate the goodness of fits, the theoretical curves obtained from the best-fit values are plotted in Figure 1 for models with $d = 6$ and $d = 8$ coefficients. Moreover, Figure 2 shows an example of the posterior probability distributions of the free parameters for GRB 130427A. The probability distributions for models with $d = 6$ and $d = 8$ coefficients are presented in the upper and lower panels of Figure 2, respectively. The corresponding distributions for other GRBs are qualitatively similar.

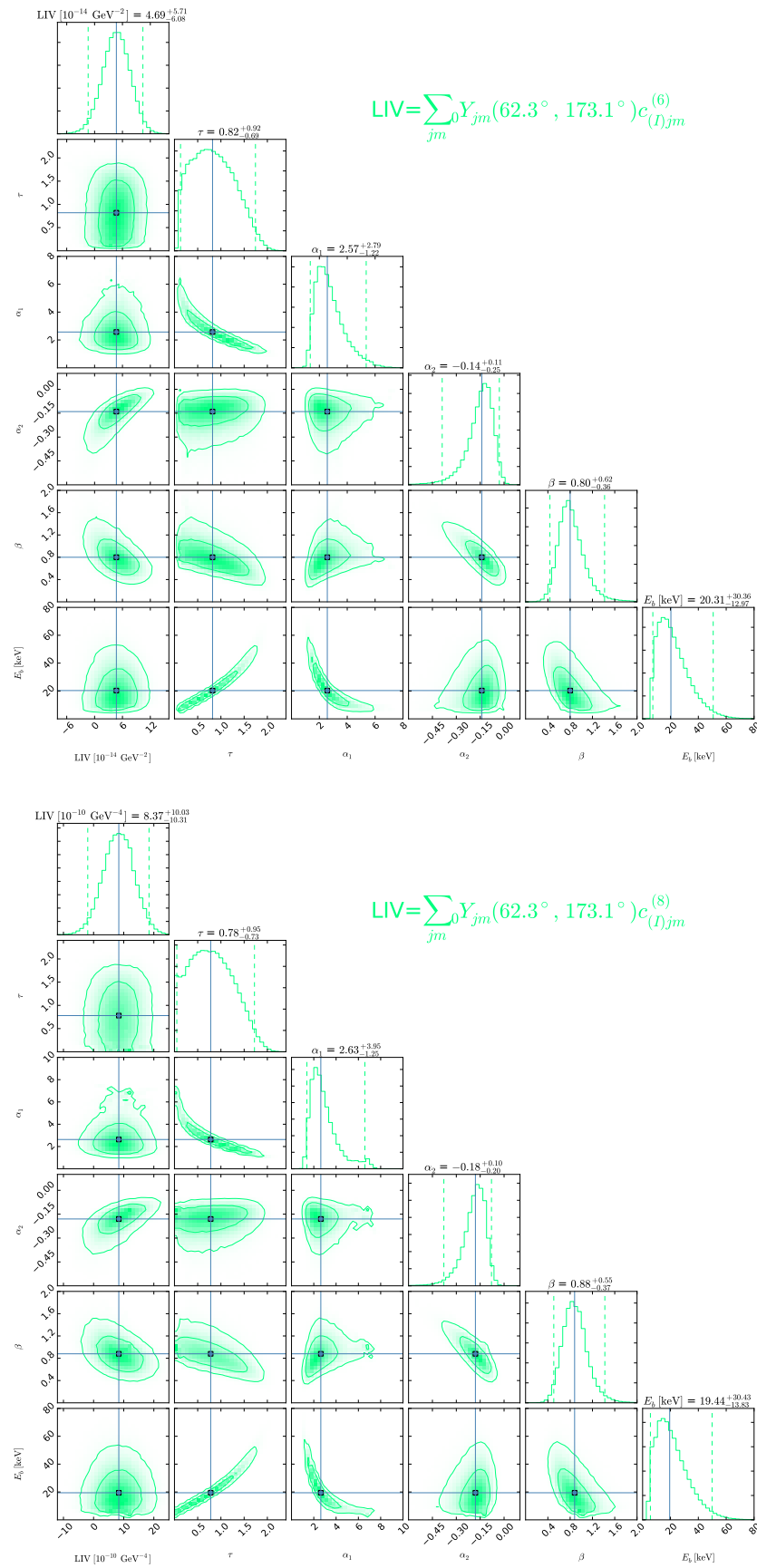**Table 2.** 95% C.L. constraints on the SME coefficients and the parameters of the SBPL function.

Name	(θ, ϕ)	d	$\sum_{jm} {}_0 Y_{jm}(\theta, \phi) c^{(d)}_{(I)jm}$ GeV^{-2} Units for $d=6$ / GeV^{-4} Units for $d=8$	$c^{(d)}_{(I)00}$ GeV^{-2} Units for $d=6$ / GeV^{-4} Untis for $d=8$	τ	α_1	α_2	E_b (keV)
GRB 080916C	$(146.6°, 119.8°)$	6	$-1.12^{+3.72}_{-2.16} \times 10^{-13}$	$-3.97^{+13.19}_{-7.66} \times 10^{-13}$	$1.52^{+0.99}_{-1.39}$	$3.61^{+4.78}_{-2.76}$	$-5.73^{+4.45}_{-3.91}$	$208.23^{+1541.98}_{-166.24}$
		8	$-1.20^{+3.94}_{-3.25} \times 10^{-8}$	$-4.25^{+13.97}_{-11.52} \times 10^{-8}$	$1.51^{+0.98}_{-1.39}$	$3.51^{+4.47}_{-2.57}$	$-5.49^{+4.21}_{-3.97}$	$219.22^{+1280.32}_{-180.51}$
GRB 081221	$(114.5°, 15.8°)$	6	$6.49^{+6.92}_{-5.58} \times 10^{-12}$	$23.01^{+24.53}_{-19.78} \times 10^{-12}$	$2.59^{+3.19}_{-2.32}$	$3.78^{+4.58}_{-2.65}$	$-4.83^{+3.87}_{-4.69}$	$11346.87^{+3412.24}_{-1269.44}$
		8	$5.19^{+5.30}_{-5.12} \times 10^{-6}$	$18.40^{+18.79}_{-18.15} \times 10^{-6}$	$1.52^{+3.69}_{-1.36}$	$3.80^{+4.99}_{-2.85}$	$-5.24^{+4.45}_{-4.40}$	$827.32^{+3793.61}_{-771.93}$
GRB 090328	$(56.6°, 155.7°)$	6	$7.46^{+6.76}_{-6.66} \times 10^{-12}$	$26.45^{+23.96}_{-23.61} \times 10^{-12}$	$2.94^{+2.87}_{-2.46}$	$2.18^{+3.50}_{-1.39}$	$-2.42^{+2.60}_{-4.65}$	$2042.26^{+2794.21}_{-1807.09}$
		8	$6.54^{+4.15}_{-4.71} \times 10^{-6}$	$23.18^{+14.71}_{-16.70} \times 10^{-6}$	$1.30^{+3.48}_{-1.04}$	$3.22^{+4.89}_{-2.47}$	$-3.93^{+4.33}_{-5.38}$	$1815.82^{+2981.54}_{-1786.95}$
GRB 090618	$(11.6°, 294.0°)$	6	$1.52^{+1.39}_{-1.27} \times 10^{-11}$	$5.39^{+4.93}_{-4.50} \times 10^{-11}$	$3.11^{+0.85}_{-2.25}$	$1.15^{+1.31}_{-0.55}$	$0.13^{+0.42}_{-1.00}$	$38.07^{+23.61}_{-31.46}$
		8	$7.14^{+7.06}_{-6.63} \times 10^{-6}$	$25.31^{+25.03}_{-23.50} \times 10^{-6}$	$3.24^{+0.73}_{-2.19}$	$1.48^{+1.27}_{-0.78}$	$-0.23^{+0.57}_{-0.91}$	$40.13^{+23.58}_{-31.24}$

Table 2. *Cont.*

Name	(θ, ϕ)	d	$\sum_{jm\,0}Y_{jm}(\theta, \phi)c^{(d)}_{(I)jm}$ GeV^{-2} Units for $d=6$ GeV^{-4} Units for $d=8$	$c^{(d)}_{(I)00}$ GeV^{-2} Units for $d=6$ GeV^{-4} Untis for $d=8$	τ	α_1	α_2	E_b (keV)
GRB 090926A	$(156.3°, 353.4°)$	6	$4.90^{+6.48}_{-5.71} \times 10^{-13}$	$17.37^{+22.97}_{-20.24} \times 10^{-13}$	$2.34^{+1.53}_{-1.88}$	$0.87^{+0.98}_{-0.42}$	$-1.70^{+1.46}_{-3.83}$	$2101.57^{+2717.75}_{-2061.80}$
		8	$8.16^{+9.12}_{-8.93} \times 10^{-8}$	$28.93^{+32.33}_{-31.66} \times 10^{-8}$	$1.94^{+1.31}_{-1.55}$	$0.96^{+0.80}_{-0.43}$	$-1.95^{+1.54}_{-2.42}$	$1777.59^{+2989.77}_{-1709.57}$
GRB 091003A	$(126.6°, 251.5°)$	6	$2.70^{+3.69}_{-2.27} \times 10^{-13}$	$9.57^{+13.08}_{-8.05} \times 10^{-13}$	$0.21^{+0.17}_{-0.18}$	$4.56^{+4.89}_{-3.38}$	$-6.74^{+5.05}_{-3.08}$	$225.55^{+1784.70}_{-152.93}$
		8	$1.14^{+1.26}_{-4.29} \times 10^{-7}$	$4.04^{+4.47}_{-4.29} \times 10^{-7}$	$0.21^{+0.17}_{-0.16}$	$4.72^{+4.83}_{-3.54}$	$-7.12^{+4.71}_{-2.73}$	$200.75^{+378.46}_{-127.32}$
GRB 100728A	$(105.3°, 88.8°)$	6	$-0.73^{+10.34}_{-5.84} \times 10^{-12}$	$-2.59^{+36.65}_{-20.70} \times 10^{-12}$	$2.61^{+1.33}_{-2.48}$	$4.75^{+4.26}_{-1.89}$	$-8.02^{+6.50}_{-347.10}$	$378.99^{+1125.68}_{-277.42}$
		8	$0.40^{+9.56}_{-5.86} \times 10^{-6}$	$1.42^{+33.89}_{-20.77} \times 10^{-6}$	$2.76^{+1.19}_{-2.13}$	$6.89^{+3.90}_{-2.90}$	$-3.23^{+3.18}_{-3.41}$	$37.79^{+14.54}_{-19.55}$
GRB 120119A	$(99.8°, 120.0°)$	6	$3.11^{+3.90}_{-3.29} \times 10^{-12}$	$11.02^{+13.83}_{-11.66} \times 10^{-12}$	$1.65^{+2.16}_{-1.57}$	$1.57^{+4.05}_{-1.04}$	$-3.33^{+2.91}_{-5.43}$	$1064.22^{+3638.78}_{-1003.59}$
		8	$1.30^{+2.05}_{-1.66} \times 10^{-6}$	$4.61^{+7.27}_{-5.88} \times 10^{-6}$	$1.22^{+2.00}_{-1.15}$	$2.17^{+4.71}_{-1.71}$	$-4.15^{+3.71}_{-4.90}$	$486.17^{+3803.39}_{-443.45}$
GRB 130427A	$(62.3°, 173.1°)$	6	$4.69^{+5.71}_{-6.08} \times 10^{-14}$	$16.63^{+20.24}_{-21.55} \times 10^{-14}$	$0.82^{+0.92}_{-0.69}$	$2.57^{+2.79}_{-1.22}$	$-0.14^{+0.11}_{-0.25}$	$20.31^{+30.36}_{-12.95}$
		8	$8.37^{+10.03}_{-10.31} \times 10^{-10}$	$29.67^{+35.56}_{-36.55} \times 10^{-10}$	$0.78^{+0.95}_{-0.73}$	$2.63^{+3.95}_{-1.25}$	$-0.18^{+0.10}_{-0.20}$	$19.44^{+30.43}_{-13.81}$
GRB 130518A	$(42.5°, 355.7°)$	6	$6.98^{+6.26}_{-5.83} \times 10^{-14}$	$24.74^{+22.19}_{-20.67} \times 10^{-14}$	$0.75^{+0.59}_{-0.41}$	$0.87^{+0.65}_{-0.37}$	$-2.24^{+1.84}_{-2.62}$	$1661.40^{+3072.03}_{-1498.65}$
		8	$4.39^{+3.32}_{-2.80} \times 10^{-9}$	$15.56^{+11.77}_{-9.93} \times 10^{-9}$	$0.64^{+0.61}_{-0.52}$	$0.90^{+0.74}_{-0.41}$	$-2.52^{+2.19}_{-2.30}$	$1353.03^{+3211.94}_{-1210.71}$
GRB 130925A	$(116.1°, 41.2°)$	6	$2.89^{+12.37}_{-7.01} \times 10^{-11}$	$10.24^{+43.85}_{-24.85} \times 10^{-11}$	$3.59^{+0.41}_{-1.67}$	$1.06^{+0.42}_{-0.21}$	$-9.46^{+1.84}_{-0.52}$	$231.66^{+151.90}_{-29.60}$
		8	$1.22^{+10.64}_{-3.59} \times 10^{-4}$	$4.32^{+37.72}_{-12.73} \times 10^{-4}$	$3.63^{+0.36}_{-2.52}$	$1.05^{+3.49}_{-0.21}$	$-9.51^{+1.68}_{-0.47}$	$226.42^{+120.21}_{-22.97}$
GRB 131108A	$(80.3°, 156.5°)$	6	$0.08^{+4.46}_{-2.91} \times 10^{-13}$	$0.28^{+15.81}_{-10.32} \times 10^{-13}$	$0.68^{+0.41}_{-0.59}$	$3.94^{+3.78}_{-2.61}$	$-6.00^{+4.66}_{-3.60}$	$331.23^{+635.92}_{-277.03}$
		8	$-3.20^{+11.17}_{-10.96} \times 10^{-8}$	$-11.34^{+39.60}_{-38.85} \times 10^{-8}$	$0.61^{+0.42}_{-0.58}$	$3.79^{+4.05}_{-2.55}$	$-6.51^{+4.23}_{-3.22}$	$346.53^{+1276.27}_{-271.00}$
GRB 131231A	$(91.6°, 10.6°)$	6	$1.04^{+0.42}_{-0.44} \times 10^{-11}$	$3.69^{+1.49}_{-1.56} \times 10^{-11}$	$3.83^{+0.16}_{-1.43}$	$1.19^{+0.99}_{-0.19}$	$0.11^{+0.17}_{-0.86}$	$32.04^{+2.56}_{-15.21}$
		8	$5.02^{+1.65}_{-1.41} \times 10^{-6}$	$17.80^{+5.85}_{-5.00} \times 10^{-6}$	$3.65^{+0.34}_{-1.61}$	$1.94^{+0.63}_{-0.61}$	$-0.58^{+0.53}_{-0.47}$	$29.89^{+4.71}_{-15.90}$
GRB 140206A	$(23.2°, 145.3°)$	6	$0.85^{+1.03}_{-0.77} \times 10^{-12}$	$3.01^{+3.65}_{-2.73} \times 10^{-12}$	$1.33^{+0.82}_{-0.74}$	$1.95^{+1.27}_{-2.58}$	$-3.06^{+2.31}_{-2.58}$	$413.97^{+2178.15}_{-390.50}$
		8	$0.57^{+0.58}_{-0.48} \times 10^{-6}$	$2.02^{+2.06}_{-1.70} \times 10^{-6}$	$1.20^{+0.68}_{-1.10}$	$2.10^{+1.22}_{-0.81}$	$-3.21^{+3.01}_{-2.86}$	$321.23^{+2120.21}_{-302.84}$
GRB 140508A	$(43.2°, 255.5°)$	6	$1.70^{+1.59}_{-1.52} \times 10^{-12}$	$6.03^{+5.64}_{-5.39} \times 10^{-12}$	$1.39^{+2.33}_{-1.26}$	$0.50^{+1.11}_{-0.26}$	$-1.28^{+1.62}_{-7.49}$	$2756.68^{+2133.35}_{-2504.72}$
		8	$0.73^{+0.73}_{-0.71} \times 10^{-6}$	$2.59^{+2.59}_{-2.52} \times 10^{-6}$	$0.74^{+1.71}_{-0.68}$	$0.45^{+1.07}_{-0.29}$	$-1.51^{+1.77}_{-6.88}$	$2388.69^{+2482.19}_{-274.19}$
GRB 141028A	$(90.0°, 322.6°)$	6	$2.13^{+4.42}_{-2.76} \times 10^{-12}$	$7.55^{+15.67}_{-9.78} \times 10^{-12}$	$2.70^{+3.11}_{-2.43}$	$3.64^{+4.71}_{-2.90}$	$-4.49^{+4.50}_{-5.02}$	$1703.81^{+3102.34}_{-1578.31}$
		8	$1.04^{+1.63}_{-1.53} \times 10^{-6}$	$3.69^{+5.78}_{-5.41} \times 10^{-6}$	$1.40^{+2.45}_{-1.26}$	$1.58^{+6.02}_{-1.15}$	$-3.41^{+3.54}_{-5.91}$	$1269.89^{+3487.24}_{-1183.83}$
GRB 150314A	$(26.2°, 126.7°)$	6	$1.25^{+2.38}_{-2.68} \times 10^{-13}$	$4.43^{+8.44}_{-1.90} \times 10^{-13}$	$2.13^{+3.58}_{-2.36}$	$2.92^{+5.40}_{-2.32}$	$-3.60^{+3.86}_{-5.85}$	$1852.58^{+2959.22}_{-1735.94}$
		8	$0.44^{+5.44}_{-3.81} \times 10^{-7}$	$1.56^{+13.51}_{-19.28} \times 10^{-7}$	$0.78^{+0.62}_{-0.42}$	$0.53^{+0.07}_{-0.15}$	$-1.97^{+1.58}_{-3.02}$	$1877.20^{+2926.92}_{-1766.16}$
GRB 150403A	$(152.7°, 311.5°)$	6	$7.14^{+8.92}_{-8.00} \times 10^{-13}$	$25.31^{+31.62}_{-28.36} \times 10^{-13}$	$2.22^{+2.02}_{-1.92}$	$0.59^{+1.10}_{-0.27}$	$-1.64^{+1.94}_{-7.24}$	$2491.52^{+637.92}_{-2182.70}$
		8	$1.94^{+1.76}_{-1.83} \times 10^{-7}$	$6.88^{+6.24}_{-6.49} \times 10^{-7}$	$1.96^{+1.87}_{-1.65}$	$0.50^{+1.02}_{-0.22}$	$-1.27^{+1.56}_{-7.51}$	$2676.79^{+2202.30}_{-2345.65}$
GRB 150514A	$(150.9°, 74.8°)$	6	$1.61^{+2.41}_{-1.56} \times 10^{-11}$	$5.71^{+8.54}_{-5.53} \times 10^{-11}$	$1.79^{+2.08}_{-1.65}$	$0.63^{+1.16}_{-0.37}$	$-1.80^{+2.15}_{-7.32}$	$2456.03^{+2411.40}_{-2284.19}$
		8	$9.66^{+9.59}_{-8.99} \times 10^{-5}$	$34.24^{+34.00}_{-31.87} \times 10^{-5}$	$1.34^{+2.41}_{-1.23}$	$0.51^{+0.95}_{-0.30}$	$-1.41^{+1.76}_{-7.49}$	$2683.10^{+2200.86}_{-2465.27}$
GRB 150821A	$(147.9°, 341.9°)$	6	$0.68^{+1.15}_{-0.61} \times 10^{-10}$	$2.41^{+4.08}_{-2.16} \times 10^{-10}$	$2.57^{+1.37}_{-1.49}$	$1.56^{+3.22}_{-0.72}$	$-4.35^{+5.28}_{-4.84}$	$1065.04^{+3724.78}_{-1051.64}$
		8	$1.69^{+1.52}_{-1.39} \times 10^{-4}$	$5.99^{+5.39}_{-4.91} \times 10^{-4}$	$3.08^{+0.88}_{-2.34}$	$2.35^{+3.84}_{-1.52}$	$-0.60^{+1.24}_{-3.14}$	$43.75^{+22.32}_{-31.84}$
GRB 160509A	$(14.0°, 310.1°)$	6	$5.57^{+11.89}_{-10.90} \times 10^{-13}$	$19.75^{+42.15}_{-38.64} \times 10^{-13}$	$1.53^{+1.20}_{-1.31}$	$0.96^{+1.51}_{-0.50}$	$-1.77^{+3.01}_{-4.02}$	$1933.51^{+2888.12}_{-1893.44}$
		8	$0.93^{+3.49}_{-3.20} \times 10^{-7}$	$3.30^{+12.37}_{-11.34} \times 10^{-7}$	$1.18^{+1.75}_{-1.02}$	$1.10^{+1.31}_{-0.64}$	$-2.19^{+2.10}_{-3.36}$	$1673.00^{+3087.91}_{-1572.41}$
GRB 160625B	$(83.1°, 308.6°)$	6	$3.63^{+0.57}_{-0.59} \times 10^{-15}$	$12.87^{+2.02}_{-2.09} \times 10^{-15}$	$0.62^{+0.18}_{-0.40}$	$2.19^{+5.19}_{-1.47}$	$0.33^{+0.03}_{-0.06}$	$64.02^{+39.56}_{-27.87}$
		8	$1.98^{+0.29}_{-0.30} \times 10^{-12}$	$7.02^{+1.03}_{-1.06} \times 10^{-12}$	$0.62^{+0.27}_{-0.43}$	$2.15^{+4.14}_{-0.96}$	$0.28^{+0.02}_{-0.03}$	$66.47^{+38.56}_{-32.10}$
GRB 171010A	$(100.5°, 66.6°)$	6	$3.45^{+4.11}_{-12.45} \times 10^{-11}$	$12.23^{+14.57}_{-44.08} \times 10^{-11}$	$3.01^{+0.97}_{-2.24}$	$1.99^{+1.38}_{-0.88}$	$-0.17^{+0.69}_{-5.96}$	$23.77^{+147.73}_{-17.42}$
		8	$2.43^{+2.58}_{-2.44} \times 10^{-5}$	$8.61^{+9.15}_{-8.65} \times 10^{-5}$	$3.04^{+0.92}_{-2.30}$	$2.39^{+1.19}_{-0.87}$	$-0.54^{+0.71}_{-0.76}$	$24.32^{+10.24}_{-17.56}$
GRB 180703A	$(157.1°, 6.5°)$	6	$2.44^{+7.37}_{-3.32} \times 10^{-12}$	$8.65^{+26.13}_{-11.77} \times 10^{-12}$	$0.84^{+0.40}_{-0.44}$	$5.84^{+3.80}_{-2.91}$	$-6.94^{+6.10}_{-110.16}$	$168.46^{+1201.15}_{-85.73}$
		8	$3.20^{+7.01}_{-5.63} \times 10^{-6}$	$11.34^{+24.85}_{-19.96} \times 10^{-6}$	$0.80^{+0.23}_{-0.54}$	$6.16^{+3.55}_{-3.73}$	$-7.05^{+6.10}_{-2.81}$	$143.70^{+257.42}_{-85.73}$
GRB 180720B	$(93.0°, 0.59°)$	6	$-0.03^{+0.70}_{-0.65} \times 10^{-14}$	$-0.11^{+2.48}_{-2.30} \times 10^{-14}$	$2.92^{+0.43}_{-1.33}$	$1.04^{+0.46}_{-0.38}$	$-0.80^{+0.66}_{-0.63}$	$2800.03^{+2092.83}_{-2465.91}$
		8	$-0.13^{+0.93}_{-0.90} \times 10^{-11}$	$-0.46^{+3.30}_{-3.19} \times 10^{-11}$	$2.95^{+0.33}_{-2.05}$	$1.06^{+0.65}_{-0.39}$	$-0.81^{+0.63}_{-0.57}$	$2785.74^{+2106.16}_{-2664.13}$
GRB 190114C	$(116.9°, 54.5°)$	6	$5.84^{+2.44}_{-2.34} \times 10^{-14}$	$20.70^{+8.65}_{-8.30} \times 10^{-14}$	$0.70^{+0.60}_{-0.61}$	$1.54^{+0.77}_{-0.57}$	$-3.04^{+1.61}_{-1.89}$	$877.77^{+3537.70}_{-810.57}$
		8	$0.97^{+0.56}_{-0.55} \times 10^{-9}$	$3.44^{+1.99}_{-1.96} \times 10^{-9}$	$0.34^{+0.94}_{-0.63}$	$1.48^{+0.70}_{-0.47}$	$-3.88^{+1.68}_{-1.77}$	$1560.07^{+3096.27}_{-1352.64}$
GRB 200613A	$(44.2°, 153.0°)$	6	$0.59^{+0.84}_{-0.72} \times 10^{-11}$	$2.09^{+2.98}_{-2.54} \times 10^{-11}$	$2.02^{+1.86}_{-1.69}$	$3.78^{+4.73}_{-3.16}$	$-4.24^{+4.12}_{-5.24}$	$1841.73^{+2983.38}_{-1748.44}$
		8	$1.21^{+1.61}_{-1.30} \times 10^{-5}$	$4.29^{+5.71}_{-5.83} \times 10^{-5}$	$1.65^{+2.18}_{-1.38}$	$3.26^{+3.82}_{-2.75}$	$-3.68^{+3.67}_{-5.75}$	$1835.19^{+2970.97}_{-1744.47}$
GRB 200829A	$(17.6°, 251.1°)$	6	$3.25^{+0.91}_{-1.06} \times 10^{-14}$	$11.52^{+3.23}_{-3.76} \times 10^{-14}$	$0.70^{+0.26}_{-0.39}$	$0.79^{+0.62}_{-0.29}$	$-1.61^{+1.22}_{-1.34}$	$2446.19^{+2432.79}_{-2406.95}$
		8	$4.40^{+2.86}_{-1.54} \times 10^{-10}$	$15.60^{+10.14}_{-5.46} \times 10^{-10}$	$0.36^{+0.45}_{-0.21}$	$0.56^{+1.61}_{-0.11}$	$-2.76^{+1.76}_{-1.74}$	$3033.55^{+1850.99}_{-2989.83}$
GRB 201216C	$(73.5°, 16.4°)$	6	$0.92^{+2.53}_{-2.52} \times 10^{-12}$	$3.26^{+8.97}_{-8.93} \times 10^{-12}$	$2.03^{+1.72}_{-2.16}$	$0.75^{+0.80}_{-0.39}$	$-1.92^{+2.06}_{-4.95}$	$1778.23^{+3002.73}_{-1764.69}$
		8	$0.08^{+1.00}_{-1.11} \times 10^{-6}$	$0.28^{+3.54}_{-3.93} \times 10^{-6}$	$1.64^{+1.55}_{-1.44}$	$0.82^{+0.88}_{-0.41}$	$-2.28^{+1.78}_{-3.35}$	$1479.39^{+3212.11}_{-1331.33}$
GRB 210204A	$(80.3°, 109.1°)$	6	$0.17^{+11.89}_{-8.90} \times 10^{-12}$	$0.60^{+42.04}_{-31.55} \times 10^{-12}$	$2.37^{+1.60}_{-2.16}$	$1.27^{+2.03}_{-0.48}$	$-3.91^{+3.87}_{-4.64}$	$308.84^{+2115.32}_{-209.90}$
		8	$0.30^{+1.40}_{-1.30} \times 10^{-5}$	$1.06^{+4.96}_{-4.61} \times 10^{-5}$	$2.77^{+1.21}_{-2.54}$	$1.30^{+2.31}_{-0.52}$	$-3.57^{+3.47}_{-4.14}$	$274.49^{+1155.77}_{-209.90}$
GRB 210610B	$(75.6°, 243.9°)$	6	$-0.77^{+10.75}_{-8.37} \times 10^{-12}$	$-2.73^{+38.11}_{-29.67} \times 10^{-12}$	$4.30^{+1.23}_{-3.87}$	$3.76^{+3.68}_{-2.68}$	$-5.72^{+5.87}_{-3.46}$	$321.33^{+1719.51}_{-287.08}$
		8	$-2.60^{+11.34}_{-11.61} \times 10^{-6}$	$-9.22^{+40.20}_{-41.16} \times 10^{-6}$	$3.94^{+1.10}_{-3.82}$	$3.88^{+3.35}_{-2.83}$	$-5.99^{+4.09}_{-3.46}$	$331.28^{+2465.18}_{-297.21}$
GRB 210619B	$(56.1°, 319.7°)$	6	$1.20^{+0.45}_{-0.46} \times 10^{-15}$	$4.25^{+1.60}_{-1.63} \times 10^{-15}$	$0.23^{+0.22}_{-0.18}$	$2.02^{+2.47}_{-0.91}$	$0.24^{+0.03}_{-0.04}$	$36.71^{+45.06}_{-23.05}$
		8	$1.52^{+0.52}_{-0.52} \times 10^{-12}$	$5.38^{+1.84}_{-1.84} \times 10^{-12}$	$0.23^{+0.23}_{-0.18}$	$2.00^{+2.33}_{-0.90}$	$0.22^{+0.03}_{-0.04}$	$36.84^{+48.26}_{-22.81}$

Figure 2. Upper panel: 1D and 2D posterior probability distributions with the 1-2σ contours for the parameters (τ, α_1, α_2, β, and E_b) and vacuum coefficients with $d = 6$ for GRB 130427A. Best-fit values

are highlighted by vertical solid lines, whereas $\pm 2\sigma$ deviations from the best-fit values are indicated by vertical dashed lines. Lower panel: same but for the analysis with $d = 8$ coefficients.

4. Discussion

Estimating from the 95% confidence levels in Table 2, most of our constraints on $\sum_{jm} {}_0 Y_{jm}(\hat{n}) c_{(I)jm}^{(d)}$ are consistent with zero within the 3σ confidence level, implying that there is no convincing evidence for LIV. However, the results from GRB 131231A, GRB 160625B, GRB 190114C, GRB 200829A, and GRB 210619B are incompatible with zero at the 4.7σ, 12.3σ, 5.0σ, 6.1σ, and 5.2σ, respectively. Given the fact that there is a significant deviation from the null hypothesis of no LIV in 5 out of 32 GRBs, here, we examine the statistical significance of the evidence for a non-zero LIV spectral lag. We fit the data to an additional hypothesis that the time lags are only due to the intrinsic astrophysical mechanisms given by Equation (6). Once we obtain the best-fit parameters, we then proceed to carry out model comparison using the Akaike Information Criterion (AIC) by treating the case of only intrinsic astrophysical emission as the null hypothesis. The AIC score of each fitted model is given as AIC $= \chi^2 + 2f$, where f is the number of model-free parameters [59,60]. With AIC_i characterizing model $\mathcal{M}_i$, the un-normalized confidence that this model is true is the Akaike weight $\exp(-\text{AIC}_i/2)$. The relative probability of $\mathcal{M}_i$ being the correct model in a one-to-one comparison is then

$$P(\mathcal{M}_i) = \frac{\exp(-\text{AIC}_i/2)}{\exp(-\text{AIC}_1/2) + \exp(-\text{AIC}_2/2)} . \tag{8}$$

It is easy to see that the model with less AIC score is the one more preferred by this criterion. According to the AIC model selection criterion, we find that compared with the LIV ($d = 6$) model, the no-LIV model can be discarded as having a probability of being correct of only $\sim 10^{-6}$ for GRB 131231A, $\sim 10^{-34}$ for GRB 160625B, $\sim 10^{-6}$ for GRB 190114C, $\sim 10^{-8}$ for GRB 200829A, and $\sim 10^{-6}$ for GRB 210619B. These results suggest that the evidence against the null hypothesis is very strong. However, the deviation of spectral-lag behavior from the SBPL model, even if present in these five GRBs, cannot be due to Lorentz-violating effects, as this would contradict with previous upper limits and must therefore be of intrinsic astrophysical origin. Since the SBPL model does not correctly describe the intrinsic lag behavior of these five GRBs, their resulting constraints on LIV can only be considered as artificial upper limits. In other words, if a more accurate model for the intrinsic lag behavior is adopted for these five GRBs, more stringent limits on LIV could be achieved.

It is worth emphasizing that most of the previous works were carried out by concentrating on the rough time lag of a single highest-energy photon and neglecting the source-intrinsic time lag. Performing a search for Lorentz-violating effects using the true multi-photon spectral-lag data and considering the intrinsic time-lag problem, as performed in this work, is therefore crucial. Although our method relies on a particular model of the GRB lag transition, our resulting constraints can still be deemed as comparatively robust.

In our analysis, we adopt the Hubble constant $H_0 = 67.36$ km s^{-1} Mpc^{-1} inferred from *Planck* cosmic microwave background observations under ΛCDM [47]. However, this value is in 5σ tension with that measured from local distance ladders ($H_0 = 73.04$ km s^{-1} Mpc^{-1}) [61]. Given the Hubble tension, we next consider whether the H_0 prior affects our constraints on the SME coefficients. We also perform a parallel analysis of the lag-energy data of GRB 130427A using a different H_0 prior. When H_0 varies from 67.36 to 73.04 km s^{-1} Mpc^{-1}, we find that the limit on the combination $\sum_{jm} {}_0 Y_{jm}(62.3°, 173.1°) c_{(I)jm}^{(6)}$ of SME coefficients varies from $4.69^{+5.71}_{-6.08} \times 10^{-14}$ GeV^{-2} to $4.62^{+5.84}_{-7.13} \times 10^{-14}$ GeV^{-2}. It is obvious that the choice of a different H_0 value has only a minimal influence on the results.

Liu et al. [25] derived limits on isotropic linear and quadratic leading-order Lorentz-violating vacuum dispersion using the same 32 GRBs. Since the linear and quadratic LIV parameters in the vacuum isotropic model are global and direction-independent, they were able to obtain the statistical distributions of the LIV parameters upon fitting the entire

sample of 32 GRBs (see Figure 3 of [25]). In this work, however, we consider anisotropic Lorentz-violating vacuum dispersion, along with direction-dependent effects. For each GRB, we derive a limit on one direction-specific combination $\sum_{jm\,0} Y_{jm}(\hat{\boldsymbol{n}}) c^{(d)}_{(I)jm}$ of Lorentz-violating coefficients. Thus, it is not feasible to conduct a global fit on the LIV parameters by taking into account all GRBs (as Liu et al. [25] carried out in their treatment) in the vacuum anisotropic model.

5. Summary

Lorentz-violating effects on the vacuum propagation of electromagnetic waves, allowing for arbitrary mass dimension d, are well described in the SME effective field theory. Operators of odd dimension d lead to both an energy-dependent vacuum dispersion and vacuum birefringence, whereas for each even d there is a subset of $(d-1)^2$ nonbirefringent Lorentz-violating operators leading to an anisotropic photon dispersion. Lorentz-violating terms with even d are characterized by a set of $(d-1)^2$ real coefficients, which can be constrained through astrophysical time-of-flight measurements from $(d-1)^2$ or more directions in the sky. In this work, we focus on measuring coefficients controlling nonbirefringent vacuum dispersion with $d=6$ and 8.

We perform a search for Lorentz-violating photon dispersion from the muti-photon spectral-lag data of 32 *Fermi* GRBs, all of whom have well-defined transitions from positive to negative spectral lags. The spectral-lag transitions can help to distinguish the possible time delay induced by Lorentz-violating effects from any source-intrinsic time delay in different energy bands. Moreover, unlike most of the previous works that rely on using the rough time lag of a single highest-energy photon, these 32 GRBs have high photon statistics, allowing the use of the true time lags of broad light curves in multi-photon bands of different energies. By fitting the spectral-lag data of 32 GRBs, we obtain robust constraints on coefficients for Lorentz violation. The results are listed in Table 2.

A compilation of existing astrophysical limits on Lorentz-violating coefficients obtained through the photon dispersion method can be found in ref. [1]. For the case of $d=6$, our constraints are not competitive with existing bounds but can be deemed as comparatively robust. For $d=8$, only a few bounds were obtained on the 49 coefficients for nonbirefringent dispersion. Our new constraints have the promise to complement existing SME constraints.

Author Contributions: Conceptualization, J.-J.W. and X.-F.W.; Formal analysis, J.-N.W.; Investigation, J.-N.W.; Methodology, Z.-K.L. and B.-B.Z.; Project administration, J.-J.W.; Software, Z.-K.L. and B.-B.Z.; Supervision, J.-J.W. and X.-F.W.; Validation, Z.-K.L. and B.-B.Z.; Writing—original draft, J.-N.W. and J.-J.W.; Writing—review & editing, B.-B.Z. and X.-F.W. All authors have read and agreed to the published version of the manuscript.

Data Availability Statement: The data underlying this article are available in the article and Liu et al. [25].

Conflicts of Interest: The authors declare no conflict of interest.

References

1. Kostelecký, V.A.; Russell, N. Data tables for Lorentz and CPT violation. *Rev. Mod. Phys.* **2011**, *83*, 11–32. [CrossRef]
2. Kostelecký, V.A.; Samuel, S. Spontaneous breaking of Lorentz symmetry in string theory. *Phys. Rev. D* **1989**, *39*, 683–685. [CrossRef] [PubMed]
3. Kostelecký, V.A.; Potting, R. CPT and strings. *Nucl. Phys. B* **1991**, *359*, 545. [CrossRef]
4. Kostelecký, V.A.; Potting, R. CPT, strings, and meson factories. *Phys. Rev. D* **1995**, *51*, 3923–3935. [CrossRef] [PubMed]
5. Mattingly, D. Modern Tests of Lorentz Invariance. *Living Rev. Relativ.* **2005**, *8*, 5. [CrossRef]
6. Amelino-Camelia, G. Quantum-Spacetime Phenomenology. *Living Rev. Relativ.* **2013**, *16*, 5. [CrossRef]
7. Tasson, J.D. What do we know about Lorentz invariance? *Rep. Prog. Phys.* **2014**, *77*, 62901. [CrossRef]
8. Wei, J.J.; Wu, X.F. Testing fundamental physics with astrophysical transients. *Front. Phys.* **2021**, *16*, 44300. [CrossRef]
9. He, P.; Ma, B.Q. Lorentz Symmetry Violation of Cosmic Photons. *Universe* **2022**, *8*, 323. [CrossRef]
10. Amelino-Camelia, G.; Ellis, J.; Mavromatos, N.E.; Nanopoulos, D.V.; Sarkar, S. Tests of quantum gravity from observations of γ-ray bursts. *Nature* **1998**, *393*, 763–765. [CrossRef]
11. Ellis, J.; Farakos, K.; Mavromatos, N.E.; Mitsou, V.A.; Nanopoulos, D.V. A Search in Gamma-Ray Burst Data for Nonconstancy of the Velocity of Light. *Astrophys. J.* **2000**, *535*, 139–151. [CrossRef]
12. Pavlopoulos, T.G. Are we observing Lorentz violation in gamma ray bursts? [rapid communication]. *Phys. Lett. B* **2005**, *625*, 13–18. [CrossRef]
13. Ellis, J.; Mavromatos, N.E.; Nanopoulos, D.V.; Sakharov, A.S.; Sarkisyan, E.K.G. Robust limits on Lorentz violation from gamma-ray bursts. *Astropart. Phys.* **2006**, *25*, 402–411. [CrossRef]
14. Jacob, U.; Piran, T. Lorentz-violation-induced arrival delays of cosmological particles. *J. Cosmol. Astropart. Phys.* **2008**, *2008*, 31. [CrossRef]
15. Kostelecký, V.A.; Mewes, M. Astrophysical Tests of Lorentz and CPT Violation with Photons. *Astrophys. J. Lett.* **2008**, *689*, L1. [CrossRef]
16. Kostelecký, V.A.; Mewes, M. Electrodynamics with Lorentz-violating operators of arbitrary dimension. *Phys. Rev. D* **2009**, *80*, 015020. [CrossRef]
17. Abdo, A.A.; Ackermann, M.; Arimoto, M.; Asano, K.; Atwood, W.B.; Axelsson, M.; Baldini, L.; Ballet, J.; Band, D.L.; Barbiellini, G.; et al. Fermi Observations of High-Energy Gamma-Ray Emission from GRB 080916C. *Science* **2009**, *323*, 1688. [CrossRef]
18. Ellis, J.; Mavromatos, N.E. Probes of Lorentz violation. *Astropart. Phys.* **2013**, *43*, 50–55. [CrossRef]
19. Vasileiou, V.; Jacholkowska, A.; Piron, F.; Bolmont, J.; Couturier, C.; Granot, J.; Stecker, F.W.; Cohen-Tanugi, J.; Longo, F. Constraints on Lorentz invariance violation from Fermi-Large Area Telescope observations of gamma-ray bursts. *Phys. Rev. D* **2013**, *87*, 122001. [CrossRef]
20. Kislat, F.; Krawczynski, H. Search for anisotropic Lorentz invariance violation with γ-rays. *Phys. Rev. D* **2015**, *92*, 045016. [CrossRef]
21. Wei, J.J.; Zhang, B.B.; Shao, L.; Wu, X.F.; Mészáros, P. A New Test of Lorentz Invariance Violation: The Spectral Lag Transition of GRB 160625B. *Astrophys. J. Lett.* **2017**, *834*, L13. [CrossRef]
22. Wei, J.J.; Wu, X.F.; Zhang, B.B.; Shao, L.; Mészáros, P.; Kostelecký, V.A. Constraining Anisotropic Lorentz Violation via the Spectral-lag Transition of GRB 160625B. *Astrophys. J.* **2017**, *842*, 115. [CrossRef]
23. Wei, J.J.; Wu, X.F. A Further Test of Lorentz Violation from the Rest-frame Spectral Lags of Gamma-Ray Bursts. *Astrophys. J.* **2017**, *851*, 127. [CrossRef]
24. Du, S.S.; Lan, L.; Wei, J.J.; Zhou, Z.M.; Gao, H.; Jiang, L.Y.; Zhang, B.B.; Liu, Z.K.; Wu, X.F.; Liang, E.W.; et al. Lorentz Invariance Violation Limits from the Spectral-lag Transition of GRB 190114C. *Astrophys. J.* **2021**, *906*, 8. [CrossRef]
25. Liu, Z.K.; Zhang, B.B.; Meng, Y.Z. Spectral Lag Transition of 32 Fermi Gamma-Ray Bursts and Their Application on Constraining Lorentz Invariance Violation. *Astrophys. J.* **2022**, *935*, 79. [CrossRef]
26. Xiao, S.; Xiong, S.L.; Wang, Y.; Zhang, S.N.; Gao, H.; Zhang, Z.; Cai, C.; Yi, Q.B.; Zhao, Y.; Tuo, Y.L.; et al. A Robust Estimation of Lorentz Invariance Violation and Intrinsic Spectral Lag of Short Gamma-Ray Bursts. *Astrophys. J. Lett.* **2022**, *924*, L29. [CrossRef]
27. Kostelecký, V.A.; Mewes, M. Cosmological Constraints on Lorentz Violation in Electrodynamics. *Phys. Rev. Lett.* **2001**, *87*, 251304. [CrossRef]
28. Kostelecký, V.A.; Mewes, M. Sensitive Polarimetric Search for Relativity Violations in Gamma-Ray Bursts. *Phys. Rev. Lett.* **2006**, *97*, 140401. [CrossRef]
29. Kostelecký, V.A.; Mewes, M. Lorentz-Violating Electrodynamics and the Cosmic Microwave Background. *Phys. Rev. Lett.* **2007**, *99*, 011601. [CrossRef]
30. Kostelecký, V.A.; Mewes, M. Constraints on Relativity Violations from Gamma-Ray Bursts. *Phys. Rev. Lett.* **2013**, *110*, 201601. [CrossRef]
31. Gubitosi, G.; Pagano, L.; Amelino-Camelia, G.; Melchiorri, A.; Cooray, A. A constraint on Planck-scale modifications to electrodynamics with CMB polarization data. *J. Cosmol. Astropart. Phys.* **2009**, *2009*, 021. [CrossRef]
32. Laurent, P.; Götz, D.; Binétruy, P.; Covino, S.; Fernandez-Soto, A. Constraints on Lorentz Invariance Violation using integral/IBIS observations of GRB041219A. *Phys. Rev. D* **2011**, *83*, 121301. [CrossRef]
33. Stecker, F.W. A new limit on Planck scale Lorentz violation from γ-ray burst polarization. *Astropart. Phys.* **2011**, *35*, 95–97. [CrossRef]

34. Toma, K.; Mukohyama, S.; Yonetoku, D.; Murakami, T.; Gunji, S.; Mihara, T.; Morihara, Y.; Sakashita, T.; Takahashi, T.; Wakashima, Y.; et al. Strict Limit on CPT Violation from Polarization of γ-Ray Bursts. *Phys. Rev. Lett.* **2012**, *109*, 241104. [CrossRef] [PubMed]

35. Kislat, F.; Krawczynski, H. Planck-scale constraints on anisotropic Lorentz and C P T invariance violations from optical polarization measurements. *Phys. Rev. D* **2017**, *95*, 083013. [CrossRef]

36. Friedman, A.S.; Leon, D.; Crowley, K.D.; Johnson, D.; Teply, G.; Tytler, D.; Keating, B.G.; Cole, G.M. Constraints on Lorentz invariance and C P T violation using optical photometry and polarimetry of active galaxies BL Lacertae and S5 B 0716 +714. *Phys. Rev. D* **2019**, *99*, 035045. [CrossRef]

37. Wei, J.J. New constraints on Lorentz invariance violation with polarized gamma-ray bursts. *Mon. Not. R. Astron. Soc.* **2019**, *485*, 2401–2406. [CrossRef]

38. Zhou, Q.Q.; Yi, S.X.; Wei, J.J.; Wu, X.F. Constraints on Lorentz Invariance Violation with Multiwavelength Polarized Astrophysical Sources. *Galaxies* **2021**, *9*, 44. [CrossRef]

39. Colladay, D.; Kostelecký, V.A. CPT violation and the standard model. *Phys. Rev. D* **1997**, *55*, 6760–6774. [CrossRef]

40. Colladay, D.; Kostelecký, V.A. Lorentz-violating extension of the standard model. *Phys. Rev. D* **1998**, *58*, 116002. [CrossRef]

41. Kostelecký, V.A. Gravity, Lorentz violation, and the standard model. *Phys. Rev. D* **2004**, *69*, 105009. [CrossRef]

42. Boggs, S.E.; Wunderer, C.B.; Hurley, K.; Coburn, W. Testing Lorentz Invariance with GRB 021206. *Astrophys. J. Lett.* **2004**, *611*, L77–L80. [CrossRef]

43. Band, D.L. Gamma-Ray Burst Spectral Evolution through Cross-Correlations of Discriminator Light Curves. *Astrophys. J.* **1997**, *486*, 928–937. [CrossRef]

44. Norris, J.P.; Nemiroff, R.J.; Bonnell, J.T.; Scargle, J.D.; Kouveliotou, C.; Paciesas, W.S.; Meegan, C.A.; Fishman, G.J. Attributes of Pulses in Long Bright Gamma-Ray Bursts. *Astrophys. J.* **1996**, *459*, 393. [CrossRef]

45. Cheng, L.X.; Ma, Y.Q.; Cheng, K.S.; Lu, T.; Zhou, Y.Y. The time delay of gamma-ray bursts in the soft energy band. *Astron. Astrophys.* **1995**, *300*, 746.

46. Kostelecký, V.A.; Mewes, M. Signals for Lorentz violation in electrodynamics. *Phys. Rev. D* **2002**, *66*, 056005. [CrossRef]

47. Planck Collaboration; Aghanim, N.; Akrami, Y.; Ashdown, M.; Aumont, J.; Baccigalupi, C.; Ballardini, M.; Banday, A.J.; Barreiro, R.B.; Bartolo, N.; et al. Planck 2018 results. VI. Cosmological parameters. *Astron. Astrophys.* **2020**, *641*, A6. [CrossRef]

48. von Kienlin, A.; Meegan, C.A.; Paciesas, W.S.; Bhat, P.N.; Bissaldi, E.; Briggs, M.S.; Burns, E.; Cleveland, W.H.; Gibby, M.H.; Giles, M.M.; et al. The Fourth Fermi-GBM Gamma-Ray Burst Catalog: A Decade of Data. *Astrophys. J.* **2020**, *893*, 46. [CrossRef]

49. Ajello, M.; Arimoto, M.; Axelsson, M.; Baldini, L.; Barbiellini, G.; Bastieri, D.; Bellazzini, R.; Bhat, P.N.; Bissaldi, E.; Blandford, R.D.; et al. A decade of gamma-ray bursts observed by Fermi-LAT: The second GRB catalog. *Astrophys. J.* **2019**, *878*, 52. [CrossRef]

50. Selsing, J.; Fynbo, J.P.U.; Heintz, K.E.; Watson, D. GRB 190114C: NOT optical counterpart and redshift. *GRB Coord. Netw.* **2019**, *23695*, 1.

51. Belkin, S.; Pozanenko, A.; Rumyantsev, V.; Volnova, A.; Mazaeva, E.; larger GRB follow-up Collaboration. GRB 200613A: CrAO optical observations. *GRB Coord. Netw.* **2020**, *28000*, 1.

52. Oates, S.R.; Kuin, N.P.M.; De Pasquale, M.; Campana, S.; Tohuvavohu, A.; Siegel, M.H.; Neil Gehrels Swift Observatory Team. GRB 200829A: Swift/UVOT-XRT photometric redshift. *GRB Coord. Netw.* **2020**, *28338*, 1.

53. Vielfaure, J.B.; Izzo, L.; Xu, D.; Vergani, S.D.; Malesani, D.B.; de Ugarte Postigo, A.; D'Elia, V.; Fynbo, J.P.U.; Kann, D.A.; Levan, A.J.; et al. GRB 201216C: VLT X-shooter spectroscopy and potential high redshift of a VHE-emitting GRB. *GRB Coord. Netw.* **2020**, *29077*, 1.

54. Xu, D.; Izzo, L.; Fynbo, J.P.U.; Kann, D.A.; Vergani, S.D.; Malesani, D.B.; Arabsalmani, M.; Rossi, A.; Pugliese, G.; Vielfaure, J.B.; et al. GRB 210204A: Redshift revision of ZTF21aagwbjr/AT2021buv (correction to GCN 29411). *GRB Coord. Netw.* **2021**, *29432*, 1.

55. de Ugarte Postigo, A.; Thoene, C.; Agui Fernandez, J.F.; Blazek, M.; Kann, D.A.; Fynbo, J.P.U.; Izzo, L.; Garcia Alvarez, D. GRB 210610B: Redshift confirmation from GTC. *GRB Coord. Netw.* **2021**, *30194*, 1.

56. de Ugarte Postigo, A.; Kann, D.A.; Thoene, C.; Blazek, M.; Agui Fernandez, J.F.; Izzo, L.; Tanvir, N.R.; Fynbo, J.P.U.; Garcia Rodriguez, A.M.; Gomez, G. GRB 210619B: Redshift from OSIRIS/GTC. *GRB Coord. Netw.* **2021**, *30272*, 1.

57. Biesiada, M.; Piórkowska, A. Lorentz invariance violation-induced time delays in GRBs in different cosmological models. *Class. Quantum Gravity* **2009**, *26*, 125007. [CrossRef]

58. Foreman-Mackey, D.; Hogg, D.W.; Lang, D.; Goodman, J. emcee: The MCMC Hammer. *Publ. Astron. Soc. Pac.* **2013**, *125*, 306. [CrossRef]

59. Akaike, H. A New Look at the Statistical Model Identification. *IEEE Trans. Autom. Control* **1974**, *19*, 716–723. [CrossRef]

60. Liddle, A.R. Information criteria for astrophysical model selection. *Mon. Not. R. Astron. Soc.* **2007**, *377*, L74–L78. [CrossRef]

61. Riess, A.G.; Yuan, W.; Macri, L.M.; Scolnic, D.; Brout, D.; Casertano, S.; Jones, D.O.; Murakami, Y.; Anand, G.S.; Breuval, L.; et al. A Comprehensive Measurement of the Local Value of the Hubble Constant with 1 km s^{-1} Mpc^{-1} Uncertainty from the Hubble Space Telescope and the SH0ES Team. *Astrophys. J. Lett.* **2022**, *934*, L7. [CrossRef]